Nuclear Instruments and Methods in Physics Research A 826 (2016) 31–38

Contents lists available at ScienceDirect

Nuclear Instruments and Methods in Physics Research A

journal homepage: www.elsevier.com/locate/nima

Characterization of a 6×6-mm^2 75-μm cell MPPC suitable for the Cherenkov Telescope Array project

G. Romeo [a,*], G. Bonanno [a], S. Garozzo [a], A. Grillo [a], D. Marano [a], M. Munari [a], M.C. Timpanaro [a], O. Catalano [b], S. Giarrusso [b], D. Impiombato [b], G. La Rosa [b], G. Sottile [b]

[a] INAF, Osservatorio Astrofisico di Catania, Via S. Sofia 78, I-95123 Catania, Italy
[b] INAF, Istituto di Astrofisica Spaziale e Fisica cosmica di Palermo, Via U. La Malfa 153, I-90146 Palermo, Italy

ARTICLE INFO

Article history:
Received 25 March 2016
Received in revised form
7 April 2016
Accepted 18 April 2016
Available online 20 April 2016

Keywords:
Silicon photomultipliers
Detector characterization
Photon Detection Efficiency
Angle of incidence

ABSTRACT

This paper presents the latest characterization results of a novel Low Cross-Talk (LCT) large-area (6×6-mm^2) Multi-Pixel Photon Counter (MPPC) detector manufactured by Hamamatsu, belonging to the recent LCT5 family and achieving a fill-factor enhancement and cross-talk reduction. In addition, the newly adopted resin coating is demonstrated to yield improved photon detection capabilities in the 290–350 nm spectral range, making the new LCT MPPC particularly suitable for emerging applications like Cherenkov Telescopes. For a 3×3-mm^2 version of the new MPPC under test, a comparative analysis of the large pixel pitch (75-μm) detector versus the smaller pixel pitch (50-μm) detector is also undertaken. Furthermore, measurements of the 6×6-mm^2 MPPC response versus the angle of incidence are provided for the characterized device.

1. Introduction

Silicon photomultipliers (SiPMs) are a relatively new class of solid-state photodetectors suitable for an increasing number of perspective applications in many scientific fields. Thanks to their outstanding characteristics in terms of photon number resolution, low operating voltage, fast dynamic response and insensitivity to magnetic fields, SiPM applications have been continuously growing over time, especially in the fields of high-energy astrophysics [1–14], nuclear medicine [15–17] and cosmic-ray muon detection [18–20].

The unique features presented by most commercially available detectors from the world's leading manufacturers are the result of modern semiconductor fabrication technologies. Considerable effort is presently being invested by the producers of SiPMs to further improve the global performance achieved by this class of devices [21–25]. In addition, the large popularity of SiPMs in the sensors community has led to a remarkable number of characterization studies and methodologies for evaluating the detector performance [26–37]. The rising demand for optimal speed and single photon time resolution on one side, and for suitable integrated front-ends on the other, has also triggered research efforts for reliable analytical investigations on the dynamic response of SiPMs, allowing a detailed analytical description of the sensor behavior [38–44].

This paper presents the characterization of a newly available large-area (6×6-mm^2) Multi-Pixel Photon Counter (MPPC) detector from Hamamatsu Photonics, addressing the challenge of high sensitivity and low cross-talk, especially requested in the new generation of Cherenkov telescopes as the ones adopted in the ASTRI Mini-Array Project [4] within the Cherenkov Telescope Array (CTA) Observatory [5,6].

We also present a comparative analysis of the large pixel pitch (75-μm) detector versus the smaller pixel pitch (50-μm) device with the same active area (3×3-mm^2), to compare the detector performance when increasing the pixel dimension for the same device size. Furthermore, to investigate the 6×6-mm^2 detector response with respect to the incident photons, measurement at several angles of incidence are provided as well.

The measurements presented here are carried out at the Catania astrophysical Observatory Laboratory for Detectors (COLD) within INAF – Osservatorio Astrofisico di Catania.

2. Large-area low cross-talk MPPC device

In the last few years, the advances in LCT technology have produced new generation MPPCs with improved characteristics and performance. New materials and processes have been adopted,

* Corresponding author.
E-mail address: giuseppe.romeo@oact.inaf.it (G. Romeo).

http://dx.doi.org/10.1016/j.nima.2016.04.060
0168-9002/

Table 1
Main physical features of the characterized large-area MPPC detector.

Device series	S13360-6075CS
Cell pitch	75 μm
Device size	6×6 mm^2
Microcells	6400
Surface coating	silicone resin
Fill-factor	82%
Breakdown voltage*	52.01 V

* At 25 °C.

achieving higher sensitivity and geometrical fill-factors. The optical trench improvement of the LCT detectors compared to the prior MPPC series of the same family is a result of new types of trenches which enables cross-talk reduction. On the other hand, the fill-factor improvement of the new MPPC series results from a functional optimization of the physical structure of the device (maximization of the active area).

The characterized large-area MPPC described in this paper belongs to the latest device series manufactured by Hamamatsu Photonics, denominated Low Cross-Talk (LCT) family and reported as the MPPC S13360 series in the manufacturer datasheet[1]. It is a prototype device provided by the vendor to the COLD laboratory for testing and evaluation purposes. Table 1 reports the main features of the characterized detector.

Moreover, silicone resin coating has been used for this device to achieve higher quantum efficiency in the near ultraviolet (NUV) spectral region. Since this kind of device is very fast and sensitive to the light in the 290–700 nm wavelength range, it is particularly suitable for the detection of Cherenkov flashes.

3. Experimental results

The electro-optical equipment used for SiPM measurements is described in [26]. The main element of the front-end electronics for SiPM characterization is the Cherenkov Imaging Telescope Integrated Read-Out Chip (CITIROC) [45–47], which is an advanced version of the Extended Analog SiPM Integrated Read-Out Chip (EASIROC) [48–51], both produced by WEEROC[2]. The modifications to CITIROC stem from INAF and originated from the design of the ASTRI SST-2M telescope camera [2,3]. To provide a versatile interface between the SiPM terminals and the CITIROC evaluation board, specific mechanical and electrical adapters have been fabricated, allowing several functional tests and measurements for SiPM characterizations to be performed. Temperature control and stabilization is obtained through a dedicated thermoelectric cooling system based on a Peltier cell; the entire cooling system is thermally calibrated and can achieve temperatures from 10 °C to 30 °C. The mechanical housing is able to host various types of detectors by simply using a dedicated electronic adapter board.

Based on the equipment mentioned above, experimental measurements on the large-area MPPC of the LCT series are presented here in terms of the main detector performance parameters, i.e. gain, dark count rate, cross-talk and Photon Detection Efficiency (*PDE*).

3.1. Gain

In order to evaluate the MPPC gain at a fixed temperature and in a specific range of operating voltages, charge amplitude histograms are produced while illuminating the SiPM detector with a LED laser source of adjustable intensity and duration. By computing the average spacing between subsequent charge peaks in terms of Analog-to-Digital Converter (ADC) channels, and scaling for the constant ADC rate (charge/channel) and amplification factor, the SiPM gain is obtained for a fixed bias condition. A detailed description of the apparatus and the adopted technique can be found in [28]. The resulting measured gain data points, as a function of the applied overvoltage (*OV*) at 25 °C are reported in Fig. 1 for the characterized detector.

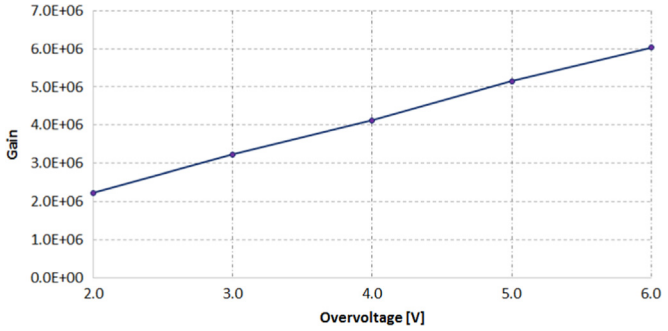

Fig. 1. Gain measurements of the characterized S13360-6075CS detector as a function of the applied overvoltage, at 25 °C.

The expected linear trend of the gain as a function of the overvoltage is observed. Gain values higher than 2×10^6 are obtained in the analyzed overvoltage range.

3.2. Dark Count Rate and cross-talk

The Dark Count Rate (*DCR*) is essentially defined as the count rate of avalanche pulses produced by primary (uncorrelated) carriers, resulting in events that are perfectly equivalent to the signal from real photons.

SiPM optical cross-talk, as reported in literature [25,27], is evaluated as the ratio of the *DCR* at 1.5 pe with respect to that at 0.5 pe. This approach is based on the assumption that the probability of triggering two uncorrelated avalanches at the same time is negligible.

Fig. 2 shows the *DCR* curves (also known as staircase functions) for the characterized LCT detector as a function of the discriminator threshold and for overvoltage values from 2.1 V up to 5.5 V, in steps of 200 mV. For a threshold above the electronics noise, all thermally generated avalanches are counted as a single pulse, as well as tunnel-assisted generated charge, afterpulsing and indirect optical cross-talk (extra-charge noise). Fig. 3 reports the measured *DCR* and cross-talk probability as a function of the overvoltage.

It can be observed that, in the analyzed overvoltage range, the *DCR* of the 6×6-mm^2 device remains lower than 700 kHz. On the other hand, for a typical 3-V overvoltage operation, the cross-talk probability is around 12%, due to the effects of the improved optical trenches adopted with respect to previous MPPC families [27].

3.3. Photon Detection Efficiency

SiPM absolute *PDE* measurements are carried out based on the photon counting method [27–29], by which the number of pulses per unit time in monochromatic light conditions are compared to the light level recorded by a reference NIST photodetector at the same time, and this process is then repeated for several wavelengths.

It is worth noting that the adopted photon counting technique for determining the detector *PDE* is insensitive to the optical cross-

[1] http://www.hamamatsu.com/jp/en/product/category/3100/4004/4113/S13360-6075CS/index.html.
[2] http://www.weeroc.com.

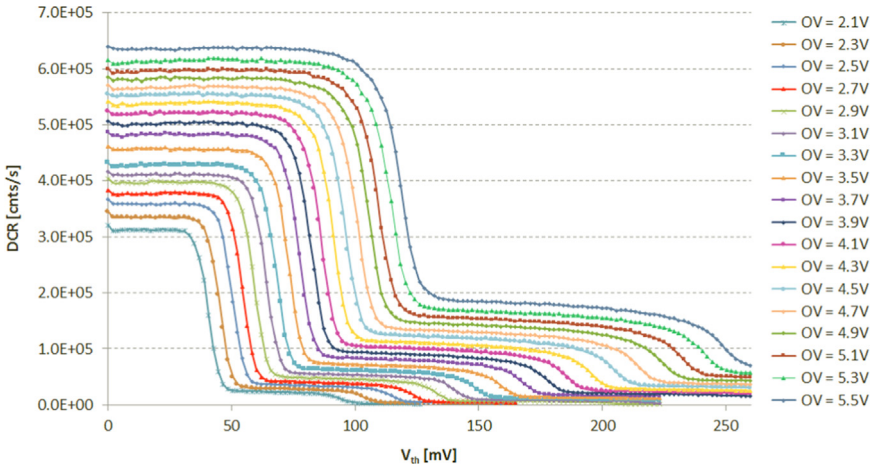

Fig. 2. Staircase measurements of the characterized S13360-6075CS detector as a function of the discriminator threshold, at 25 °C.

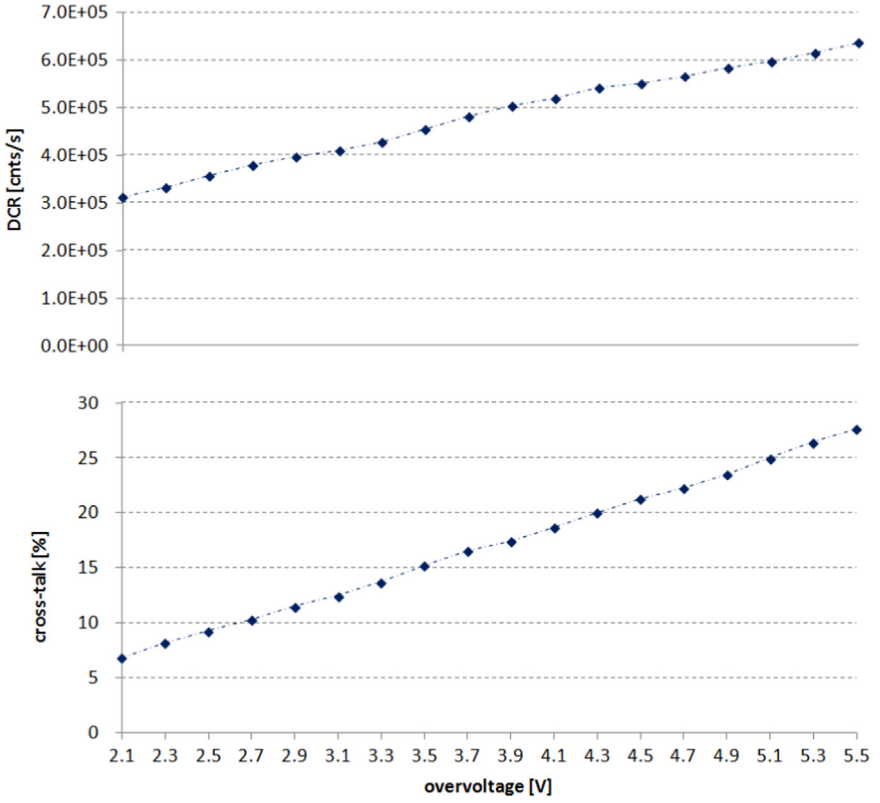

Fig. 3. *DCR* and cross-talk of the characterized S13360-6075CS detector as a function of the overvoltage, at 25 °C.

talk, as a 0.5-pe threshold is applied to all triggered pulses, so that simultaneous pulses are measured as a single pulse. However, the obtained *PDE* results are not immune to extra-charge noise (indirect cross-talk and afterpulsing), and therefore may be slightly overestimated.

PDE measurements in the 250–1000-nm wavelength range are reported in Fig. 4. The 290–350-nm range is particularly important in applications to detect Cherenkov light.

The detector *PDE* at a 450-nm wavelength as a function of the applied overvoltage is shown in Fig. 5. For rising overvoltage values, a *PDE* of almost 50% can be obtained but, of course, at the expense of an increase in cross-talk; furthermore, a progressive reduction in the *PDE* increase is observed at overvoltages higher than 3.5 V.

In order to better quantify the detector performance, *PDE* measurements at 450 nm as a function of cross-talk are reported in Fig. 6. Such a plot allows an evaluation of the optimal trade-off between *PDE* and cross-talk for the specific application. Data points in Fig. 6 refer to the same overvoltage values as in Fig. 5.

3.4. 50-μm vs. 75-μm pixel pitch LCT MPPCs

For a specific MPPC application, it is also important to evaluate the optimal trade-off between the detector *PDE* and cross-talk with respect to the pixel pitch. In fact, larger micro-pixels (better MPPC fill factor) means higher *PDE* but also implies a slightly increase in cross-talk probability. For these reasons, a comparative analysis of the large pixel pitch (75-μm) detector compared to the smaller (50-μm) device for the same active area is believed to be particularly important.

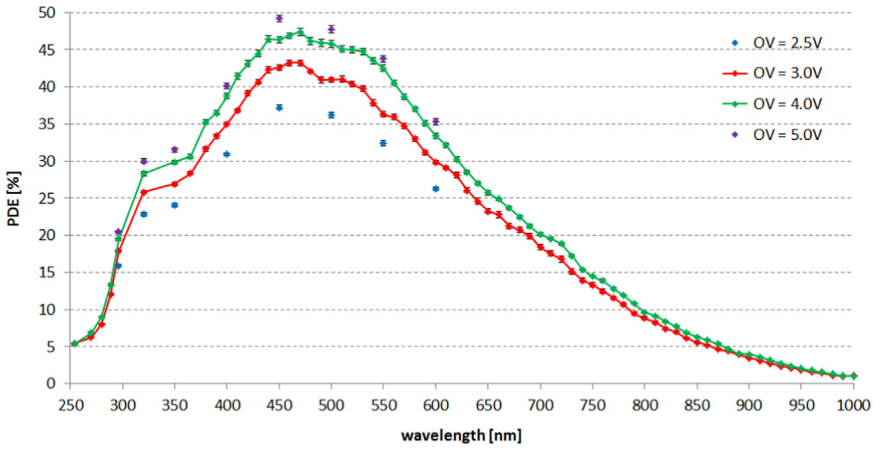

Fig. 4. *PDE* measurements of the characterized S13360-6075CS detector at various overvoltages. Measurements at 3-V and 4-V overvoltage are carried out in the 250–1000 nm spectral range in steps of 10 nm, while only eight points are shown for the other overvoltages.

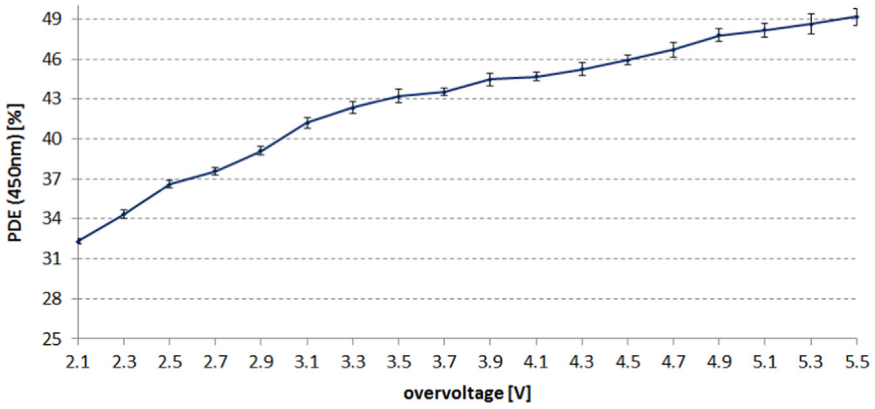

Fig. 5. *PDE* (450 nm) versus the applied overvoltage for the S13360-6075CS detector.

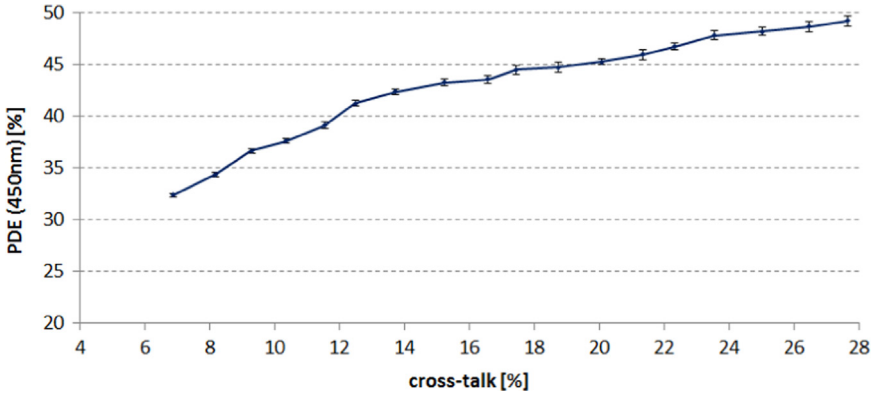

Fig. 6. *PDE* (450 nm) versus the cross-talk for the S13360-6075CS detector.

As a large-area LCT MPPC with a 50-μm pixel pitch is not presently available in our laboratory, the comparison is carried out using the 3×3-mm^2 detectors. Fig. 7 depicts the *PDE* (450 nm) curves as a function of the applied overvoltage for two 3×3-mm^2 MPPCs of the S13360 series and, in particular, the S13360-3075CS device, with a 75-μm cell size, and the S13360-3050CS counterpart, with a 50-μm active area. As can be noted, at overvoltages higher than 3.5 V, the 75-μm pitch MPPC presents a *PDE* value that is between 8% and 9% higher than that of the 50-μm pitch detector, which is compatible with the difference in fill factor of the two devices (82% for the 75-μm detector against 74% for the 50-μm device). The difference in *PDE* between the two MPPCs gradually decreases at overvoltages lower than 3 V. A better and more significant comparison is given by the *PDE* plots (at a wavelength of 450 nm) in Fig. 8 as a function of the cross-talk.

As can be observed comparing the two curves, while the S13360-3050CS MPPC is characterized by a lower cross-talk in the 30–40% *PDE* range, the S13360-3075CS device gives a higher *PDE* at greater cross-talk values. The two MPPCs present almost the same *PDE* value (39.5%) at a cross-talk of 8.5%. In applications where a cross-talk of ~20% is acceptable, a *PDE* of about 48% can be achieved only by the S13360-3075CS device. On the other hand,

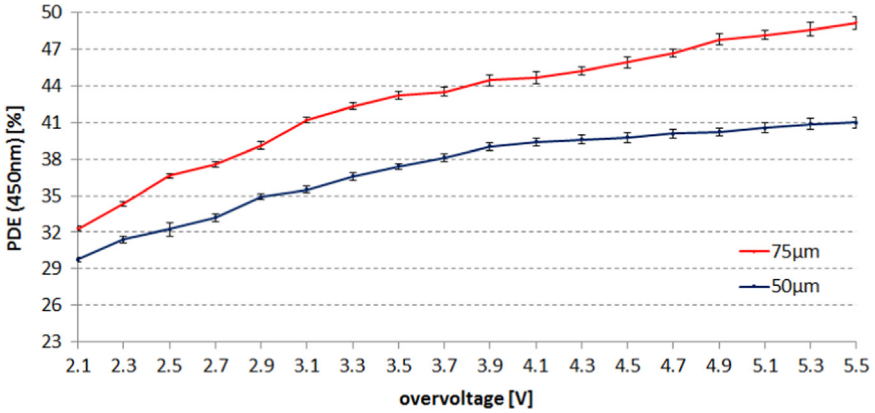

Fig. 7. *PDE* (450 nm) of the 50-µm and 75-µm LCT detectors as a function of the applied overvoltage.

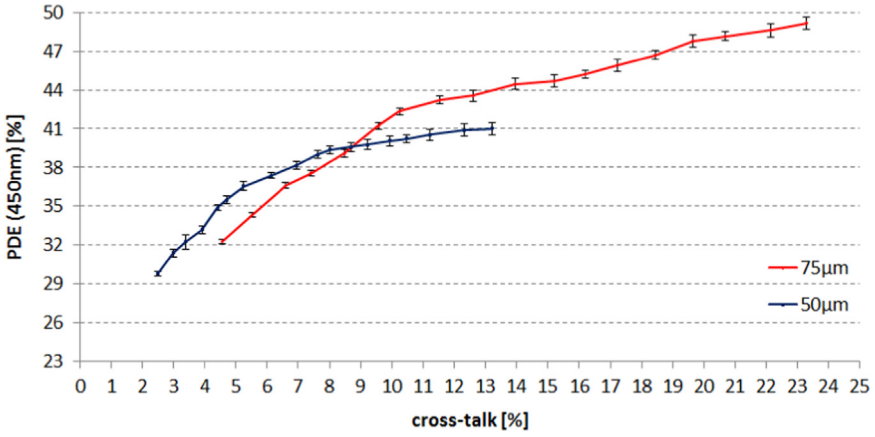

Fig. 8. *PDE* (450 nm) versus the cross-talk for the 50-µm and 75-µm LCT detectors.

the 50-µm pitch device is preferable where low cross-talk values are required.

4. Response versus angle of incidence measurements

In this section, the 6×6-mm^2 MPPC response versus the incidence radiation angle is addressed.

4.1. Measurement set-up

Measurements of the MPPC Photon Response (*PR*) versus the Angle of Incidence (*AoI*) have been performed using the experimental set-up illustrated in Fig. 9.

It consists of a PSAU-SiPM assembly [28], a light source with a high degree of uniformity and a 2-m long PVC cylindrical light-tight enclosure. The source is a green LED (568-nm wavelength), feeding a Labsphere standard integrating sphere (mod. IS-080, 8-in. diameter), that gives a uniform irradiance at the output port.

To obtain a collimated beam we introduced two diaphragms of 5 cm diameter along the tube. Taking into account the presence of these diaphragms, the length of the tube and the MPPC dimensions (6×6 mm^2), the beam divergence is lower than 1° (see Fig. 10).

The PSAU-SiPM assembly is mounted on a mechanical system (see Fig. 11) that allows the rotation of the SiPM around an axis parallel to the surface of the sensor and aligned with its center, obtaining a variation of the *AoI* of the beam with the detector. The rotary stage (OWIS DMT40-D20-HSM) can be controlled via

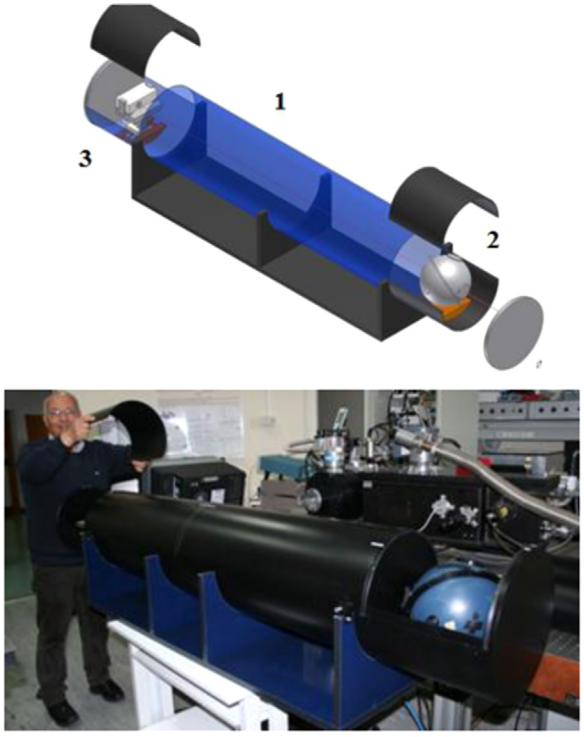

Fig. 9. Experimental set-up for the angle of incidence measurements. In the upper panel, a 3D view of the system: 1. the tube; 2. source and integrating sphere; 3. the PSAU-CAEN system. In the lower panel, photograph of the actual system.

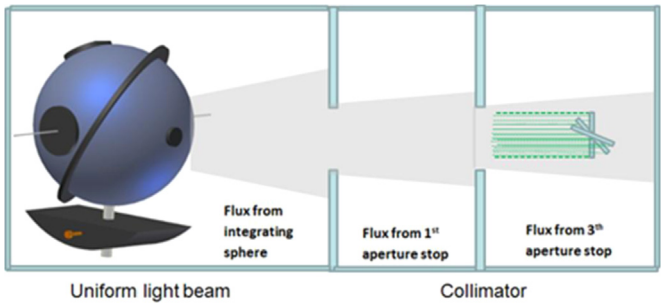

Fig. 10. Schematic of the beam collimation system.

Fig. 11. Scheme of the PSAU-SiPM system mounted on stages (upper panel, 3D view of the rotary system; lower panel, photograph of the actual apparatus, showing the realized spot pointing at the detector surface).

computer, and permits a positional accuracy of 1/10 of a degree (from the manufacturer datasheet).

The correct positioning of the SiPM with respect to the axis of rotation is assured by the presence of three linear stages that allow the translation of the SiPM itself: a laser beam is used to produce a spot on the surface of the detector and the linear stages are moved, checking that in rotating the system the spot does not move.

A fan mounted behind the PSAU-SiPM system ensures the removal/dispersal of the excess heat generated by the PSAU electronics.

4.2. Measurement results

Once the system is mounted, the first operation is to define a raw zero position of the rotary stage. Due to the set-up geometry, the signal will have a cosine-like dependence on the *AoI*. Hence, the zero point of *AoI* (detector perpendicular to the beam) is defined as the rotary stage position for which a maximum signal is recorded.

The second step was to record the *DCR* at 0.5 pe when the source was switched off. The *DCR* has been measured not only at the zero position, but also at different positions of the rotary stage: this has been done to take into account contributions to the signal due to light leakages in the enclosure. To guarantee stability of the LED emission, and thus avoid signal fluctuations, the source is turned-on one hour before measurements.

The raw signal $RS(\theta)$ and dark signal $DCR(\theta)$ have been recorded for each angular position θ of the rotary stage, with θ ranging from $-20°$ to $+75°$, in steps of 5°; The positive direction is arbitrary.

It should be noted that both $RS(\theta)$ and $DCR(\theta)$ are actually the mean values of 15 measurements and their σ_{RS} and σ_{DCR} correspond to the rms respect to the average.

From each pair of $RS(\theta)$ and $DCR(\theta)$ a net signal $SN(\theta)$ has been calculated as:

$$SN(\theta) = RS(\theta) - DCR(\theta) \tag{1}$$

The error on $SN(\theta)$ has been estimated as:

$$\sigma_{SN} = \sqrt{\sigma_{RS}^2 + \sigma_{DCR}^2} \tag{2}$$

Since, as stated before, the measurements are expected to follow a cosine trend, they can be fit with a function of the form:

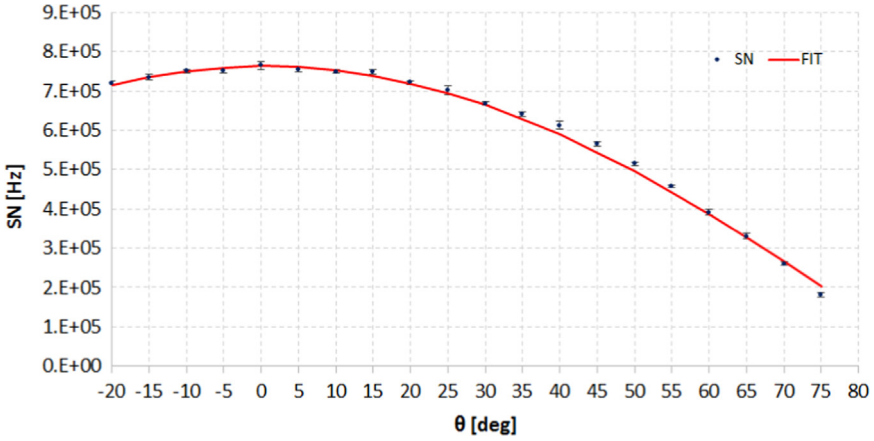

Fig. 12. Detected signal SN at 568 nm vs incidence angles (dark-blue points). The best fit model is plotted with the red line. Parameters of the fit are SN_0=7.653E5 ± 5E2 counts/s, and θ_0=-0.69 ± 0.06°. Error bars correspond to $\pm 3\sigma_{SN}$. (For interpretation of the references to color in this figure legend, the reader is referred to the web version of this article.)

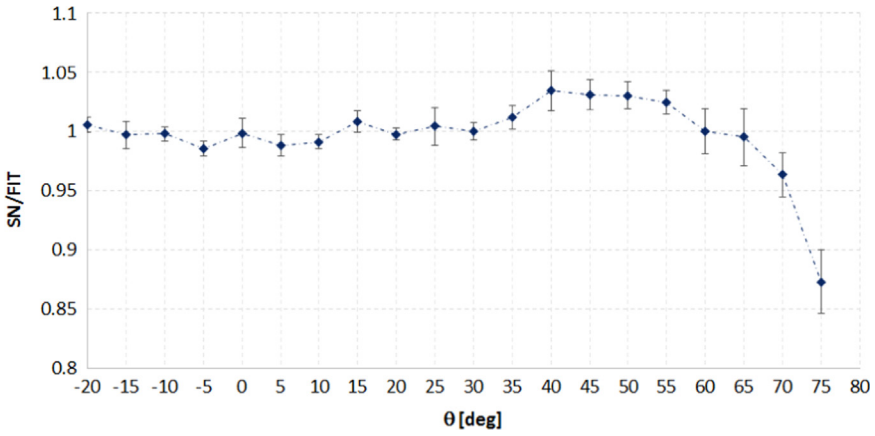

Fig. 13. Plot of the ratio *SN*/*FIT*.

$$FIT(\theta) = SN_0 \cos(\theta + \theta_0) \tag{3}$$

where θ_0 is the offset error in identifying the zero position of the rotary stage and SN_0 is the value at the zero angle of the net signal. We are assuming here that the error affecting the positioning of the angular stage is small with respect to θ_0.

SN_0 and θ_0 have been estimated using a Python MPFIT routine from the *astrolibpy* library[3], and the results of the fit (*FIT*) can be seen in the plot reported in Fig. 12.

An optimal agreement is evident in the figure.

In order to highlight the small differences between the measured data and the obtained *FIT*, we calculated, point-by-point, the ratio of the net signal over the fit values by the formula:

$$R_i = \frac{SN_i}{FIT_i} \tag{4}$$

and we also evaluated the error on each value of *R* as:

$$\sigma_{RS} = \frac{\sigma_{SN}}{FIT_i} \tag{5}$$

The *R* values are plotted in Fig. 13, where the error bars are $\pm 3\sigma$.

As shown in the plot, once the cosine dependency has been accounted for, the detector response remains constant (within few percent variation) up to 35°, slightly increases in the 35–60° range and drops down to 85% of the initial value at 75°.

Surprisingly, while a decrease of *R* for high angles may be foreseen, given the low efficiency of the anti-reflection (AR) feature of the silicone resin coating for such angles, an increase (even if always limited in a 3% range) can be noted for angles between 35° and 55°. This trend has been confirmed in several measurements and, in our opinion, can be attributed both to the presence of spurious reflections from parts of the enclosure or from the CAEN box and to mechanical effects (e.g. misalignment of the rotation axis with respect to detector plane, non-linearity of stage motion, etc.). It should be noted that the application of black screens and foils has not reduced this effect. A possible different reason can be the variation of the AR coating efficacy with the angle of incidence. All these effects will be investigated more carefully in future works.

5. Conclusions and outlook

In this paper, measurement results of a newly available large-area MPPC detector (S13360-6075CS) are reported and discussed. Compared to previous LCT MPPC series, the new LCT device achieves a significant cross-talk reduction due to optical trench improvements, and higher Photon Detection Efficiency, due to geometrical fill-factor enhancement. In addition, it offers improved photon detection capabilities in the NUV spectral region, contributing to make this new MPPC particularly suitable for new and challenging applications like CTA. Measurement results show that, even for large area devices, promising performance is achieved as well as for the 3×3-mm^2 MPPCs. Finally, measurements of the MPPC photon response versus the angle of incidence are also reported.

[3] http://code.google.com/p/astrolibpy/source/browse/trunk.

Acknowledgments

This work was supported in part by the ASTRI Flagship Project, financed by the Italian Ministry of Education, University, and Research (MIUR) and led by the Italian National Institute for Astrophysics (INAF). We gratefully acknowledge support from the agencies and organizations listed in http://www.cta-observatory.org/?q=node/22.

References

[1] D. Marano, et al., Electro-optical characterization of MPPC detectors for the ASTRI Cherenkov telescope camera, Nucl. Instrum. Methods Phys. Res. A 768 (2014) 32–42.
[2] G. Pareschi, et al., The dual-mirror small size telescope for the cherenkov telescope array, in: Proceedings of ICRC '13, Rio De Janeiro, Brazil, 2013.
[3] O. Catalano et al., The camera of the ASTRI SST-2M prototype for the cherenkov telescope array, in: Proceedings of SPIE '14, Ground-based and Airborne Instrumentation for Astronomy V 91470D, Montreal Canada, 2014.
[4] S. Vercellone, et al., The ASTRI miny-array science case, in: Proceedings of ICRC 2013, Rio De Janeiro, Brazil, July 2013.
[5] O. Catalano, et al., The ASTRI SST-2M prototype: camera and electronics, in: Proceedings of ICRC '13, Rio de Janeiro, 2013.
[6] B.S. Acharya, et al., Introducing the CTA concept, Astropart. Phys. 43 (2013) 3–18.
[7] A. Bouvier et al., Photosensor characterization for the cherenkov telescope array: silicon photomultiplier versus multi-anode photomultiplier tube, in: Proceedings of SPIE, Hard X-Ray, Gamma-Ray, and Neutron Detector Physics XV, vol. 8852, San Diego USA, 2013.
[8] H. Anderhub, et al., A novel camera type for very high energy gamma-ray astronomy based on Geiger-mode avalanche photodiodes, J. Instrum. 4 (2009) P10010.
[9] H. Anderhub, et al., Design and operation of FACT – the first G-APD Cherenkov telescope, J. Instrume. 8 (2013) P06008.
[10] A. Biland, et al., Calibration and performance of the photon sensor response of FACT – the first G-APD Cherenkov telescope, J. Instrum. 9 (2014) P10012.
[11] D. Mazin et al., Towards SiPM camera for current and future generations of Cherenkov telescopes, in: Proceedings of ICRC '13, Rio De Janeiro, Brazil, 2013.
[12] A. Biland, et al., First detection of air shower Cherenkov light by Geigermode-

avalanche photodiodes, Nucl. Instrum. Methods Phys. Res. A 595 (1) (2008) 165–168.
[13] N. Otte, et al., The potential of SiPM as photon detector in astroparticle physics experiments like MAGIC and EUSO, Nucl. Phys. B – Proc. Suppl. 50 (2006) 144–149.
[14] G. Sottile, et al., UVSiPM: a light detector instrument based on a SiPM sensor working in single photon counting, Nucl. Phys. B – Proc. Suppl. 239 (2013) 258–261.
[15] P. Buzhan, et al., Silicon photomultiplier and its possible applications, Nucl. Instrum. Methods Phys. Res. A 504 (2003) 48–52.
[16] S. Siefert et al., Ultra precise timing with SiPM-Based TOF PET scintillation detectors, in: Proceedings of IEEE Nuclear Science Symposium Conference Records, 2009, pp. 2329–2333.
[17] N. Otte, et al., The SiPM – a new photon detector for PET, Nucl.Phys. B – Proc. Suppl. 50 (2006) 417–420.
[18] P. La Rocca, et al., Fabrication, characterization and testing of silicon photomultipliers for the muon portal project, Nucl. Instrum. Methods Phys. Res. A 787 (2015) 236–239.
[19] F. Riggi, An extensive air shower trigger station for the muon portal detector, Nucl. Instrum. Methods Phys. Res. A 764 (2014) 142–149.
[20] O. Catalano, et al., Volcanoes muon imaging using cherenkov telescopes, Nucl. Instrum. Methods Phys. Res. A 807 (2016) 5–12.
[21] C. Piemonte, et al., Characterization of the first prototypes of silicon photomultiplier fabricated at ITC-irst, IEEE Trans. Nucl. Sci. 54 (1) (2007) 236–244.
[22] K. O'Neill, et al., SensL B-series and C-series silicon photomultipliers for time-of-flight positron emission tomography, Nucl. Instrum. Methods Phys. Res. A 787 (1) (2015) 169–172.
[23] B. Dolgoshein, et al., Large area UV SiPMs with Extremely low cross-talk, Nucl. Instrum. Methods Phys. Res. A 695 (2012) 40–43.
[24] C. Jendrysik, et al., Characterization of the first prototypes of silicon photomultipliers with bulk-integrated quench resistor fabricated at MPI, Nucl. Instrum. Methods Phys. Res. A 718 (2013) 262–265.
[25] V. Boccone, et al., Characterization of new hexagonal large-area geiger avalanche Photodiodes, Proc. IEEE ANIMMA (2013) 1–6.
[26] G. Bonanno, et al., Advances in multi-pixel photon counter technology: first characterization results, Nucl. Instrum. Methods Phys. Res. A 806 (2016) 383–394.
[27] G. Bonanno, et al., Characterization measurements methodology and instrumental set-up optimization for new SiPM detectors – Part II: optical tests, IEEE Sens. J. 14 (10) (2014) 3567–3578.
[28] G. Bonanno, et al., Characterization measurements methodology and instrumental set-up optimization for new SiPM detectors – Part I: electrical tests, IEEE Sens. J. 14 (10) (2014) 3557–3566.
[29] P. Eckert, et al., Characterisation studies of silicon photomultipliers, Nucl. Instrum. Methods Phys. Res. A 620 (1) (2010) 217–226.
[30] G. Bonanno, et al., Precision measurements of photon detection efficiency for SiPM detectors, Nucl. Instrum. Methods Phys. Res. A vol. 610 (2009) 93–97.
[31] S.K. Yang, et al., Precision measurements of the photon detection efficiency of silicon photomultipliers using two integrated spheres, Opt. Express 22 (1) (2014) 716–726.
[32] O. Soto, et al., Characterization of novel hamamatsu multi pixel photon counter (MPPC) arrays for the GlueX experiment, Nucl. Instrum. Methods Phys. Res. A 732 (2013) 431–436.
[33] K. Doroud, et al., Systematic study of new types of hamamatsu MPPCs read out with the NINO ASIC, Nucl. Instrum. Methods Phys. Res. A 753 (2014) 149–153.
[34] A. Vacherect, et al., Characterization and simulation of the response of multi-pixel photon counters to low light levels, Nucl. Instrum. Methods Phys. Res. A 656 (1) (2011) 69–83.
[35] P. Buzhan, et al., The cross-talk problem in SiPMs and their use as light sensors for imaging, Nucl. Instrum. Methods Phys. Res. A 610 (2009) 131–134.
[36] G. Bonanno, et al., Geiger avalanche photodiodes (G-APDs) and their characterization, photodiodes, ISBN: 978-953-307-530-3, InTech, World Activities in 2011.
[37] D. Impiombato, et al., Evaluation of the optical cross-talk level in the SiPMs adopted in ASTRI-SST-2M cherenkov camera using EASIROC front-end electronics, J. Instrum. 9 (2014) C02015.
[38] D. Marano, et al., New improved model and accurate analytical response of SiPMs coupled to read-out electronics, IEEE Sens. J. 16 (1) (2016) 17–21.
[39] F. Villa, et al., SPICE electrical models and simulations of silicon photomultipliers, IEEE Trans. Nucl. Sci. 62 (5) (2015) 1950–1960.
[40] D. Marano, et al., Accurate analytical single-photoelectron response of silicon photomultipliers, IEEE Sens. J. 14 (8) (2014) 2749–2754.
[41] D. Marano, et al., Silicon photomultipliers electrical model extensive analytical analysis, IEEE Trans. Nucl. Sci. 61 (1) (2014) 23–34.
[42] D. Marano, et al., Improved SPICE electrical model of silicon photomultipliers, Nucl. Instrum. Methods Phys. Res. A 726 (2013) 1–7.
[43] S. Vinogradov, et al., SiPM response to long and intense pulses, Nucl. Instrum. Methods Phys. Res. A 787 (2015) 148–152.
[44] I. Rech, et al., Optical crosstalk in single photon avalanche diode arrays: a new complete model, Opt. Express 16 (12) (2008) 8381–8394.
[45] J. Fleury, et al., Petiroc and citiroc: front-end ASICs for SiPM read-out and ToF applications, J. Instrum. 9 (1) (2014).
[46] D. Marano, et al., CITIROC high-level analog front-end model implementation and simulations, Int. J. Circuits Syst. Signal Process. 8 (2014) 274–285.
[47] D. Impiombato, et al., Characterization and performance of the ASIC (CITIROC) front-end of the ASTRI camera, Nucl. Instrum. Methods Phys. Res. A 794 (2015) 185–192.
[48] S. Callier, et al., EASIROC, an easy & versatile readout device for SiPM, Proc. TIPP (2001).
[49] D. Marano, et al., PSPICE high-level model and simulations of the EASIROC analog front-end, Int. J. Model. Simul. 34 (4) (2015).
[50] D. Impiombato, et al., Characterization of EASIROC as front-end for the read-out of the SiPM at the focal plane of the cherenkov telescope ASTRI, Nucl. Instrum. Methods Phys. Res. A 729 (2013) 484–490.
[51] D. Impiombato, et al., Characterization of the front-end EASIROC for read-out of SiPM in the ASTRI camera, Nucl. Phys. B-Proc. Suppl. 239 (2013) 254–257.